Fizika Nizkikh Temperatur, 2002, v. 28, No. 7, p. 733 –738

Nonlinear optical spectroscopy of epitaxial magnetic garnet films

V. V. Pavlov and R. V. Pisarev

A. F. Ioffe Physical Technical Institute of the Russian Academy of Sciences, St. Petersburg, 194021 Russia
E-mail: pisarev@pop.ioffe.rssi.ru

M. Fiebig and D. Fröhlich

Institut für Physik, Universität Dortmund, 44221 Dortmund, Germany

Received February 1, 2002

Second and third harmonic optical spectra are studied in epitaxial magnetic thin films in the spectral ranges 1.7–3.2 eV and 2.4–4.2 eV, respectively. No significant increase of the intensity of the nonlinear spectra is found above the bandgap near 3.2 eV, where the linear absorption increases by two orders of magnitude. Large magnetic contributions to the second harmonic spectra and magnetic contrast as high as 100% are observed at selected photon energies. Contrary to that, no magnetic contribution to the third harmonic spectra is found.

PACS: **78.20.–e**, 42.65.Ky, 75.50.Gg

1. Introduction

Bulk magnetic garnets and epitaxial magnetic garnet films are two well-known groups of materials characterized by a large variety of very useful magnetic, acoustic, optical, and magneto-optical properties [1–4]. For more than four decades they have remained one of the most actively studied magnetic dielectrics, both from the fundamental point of view as multi-sublattice ferrimagnets and for the purpose of technological applications. The prototype material of bulk crystals and thin films is yttrium iron garnet $\{Y\}_3[Fe]_2(Fe)_3O_{12}$ (YIG). The unit cell contains eight formula units. The rare-earth ions R^{3+} enter 24*c* dodecahedral positions $8\{\ldots\}_3$, while the Fe^{3+} ions enter 16*a* octahedral positions $8[\ldots]_2$ and 24*d* tetrahedral positions $8(\ldots)_3$. The superexchange interaction between the magnetic Fe^{3+} ions leads to antiparallel ferrimagnetic ordering of the magnetic moments of the octahedral and tetrahedral iron sublattices. This strong interaction leads to a Curie temperature in the range of $T_C = 500–600$ K. The superexchange interaction between the rare-earth magnetic ions and the iron sublattices leads to an antiparallel orientation of the rare-earth magnetic moments with respect to the magnetization of the tetrahedral sublattice. A remarkable feature of magnetic garnets is the possibility of substituting ions in all three magnetic sublattices by many other magnetic and nonmagnetic ions from the periodic table of the elements. This degree of freedom allows one to vary practically all of the physical properties of bulk crystals and epitaxial films over a very wide range.

The magnetic iron garnets are highly transparent in the near infrared range 0.2–1.0 eV [5]. At lower energy the absorption rapidly increases due to lattice vibrations. The absorption increases progressively at photon energies higher than about 1 eV due to the intrinsic localized electronic transitions between the $(3d)^5$ levels of the Fe^{3+} ions and, subsequently, above 3.2 eV due to intense charge-transfer and interband transitions, finally approaching absorption coefficients as high as $5 \cdot 10^5$ cm^{-1} above 5 eV [6]. The linear magneto-optical properties of garnets, and in particular bismuth-substituted garnets, have attracted a lot of interest due to the fact that very high values of the specific Faraday rotation up to 10^5 deg/cm were observed at room temperature. To our knowledge, these values are probably the highest ever observed at room temperature due to a spontaneous magnetization.

Bulk crystals of magnetic garnets belong to the centrosymmetric cubic point group $m3m$ (space group $Ia3d$). In the thin films, however, the observation of a linear magneto-electric effect proved that the inversion symmetry is broken [7]. This is related to the fact that the films, which are grown by a liquid-phase epitaxial method on substrates cut from bulk cubic crystals of gadolinium gallium garnet $Gd_3Ga_5O_{12}$ (GGG) or substituted GGG (SGGG), possess a lattice parameter different from that of the substrate, which leads to a distorted noncubic crystal structure. Previous studies of second harmonic generation (SHG) in magnetic garnet films were restricted to a few selected photon energies determined by the pump lasers, such as 1.17 eV (Nd:YAG lasers) or ≃ 1.5 eV (Ti–sapphire lasers) [8]. Though breaking of inversion is not important in the analysis of the magnetic properties, it plays an essential role for the electro-optical and nonlinear optical properties. In particular, it allows crystallographic and the magnetic contributions to SHG in the electric dipole approximation. Obviously, studies at selected photon energies could not clarify relations between observed SHG signals and particular features of electronic structure, absorption spectra and magneto-optical spectra. In the present paper we report first results on a spectroscopic study of SHG and third harmonic generation (THG) in magnetic garnet films below and above the fundamental band gap near 3.2 eV.

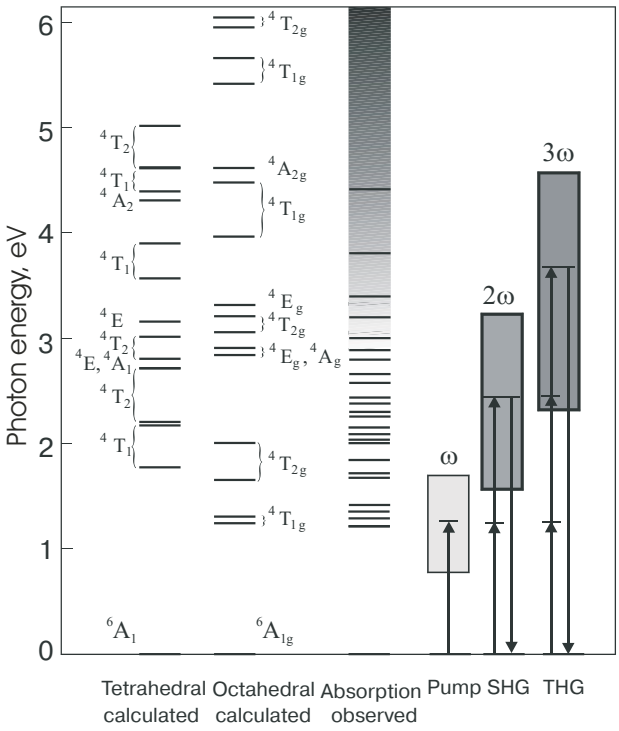

Fig. 1. The two columns on the left show the crystal field energy states of the Fe^{3+} ion in the distorted tetrahedral and octahedral positions in the garnet structure. The column in the middle shows the experimentally observed electronic transitions and the continuous absorption at higher photon energy. The right part of the figure shows the energy range of the pump beam and that of the SH and TH spectra.

2. Electronic transitions in iron garnets

Optical absorption and reflection spectra of concentrated and diluted iron garnets have been studied in a large number of publications and the most important data are summarized in Ref. 4. In spite of numerous publications along these lines, the assignments of spectral features remain doubtful in most cases due to the complexity of the spectra. Experimental data and crystal field calculations are summarized in Fig. 1. In its middle part Fig. 1 shows experimentally observed transition energies in YIG as reported in several papers [5,6,9–15]. The electronic structure of iron garnets has been a subject of calculations based on crystal field theory and molecular orbital theory [5,9,14,16–18]. The left panels of Fig. 1 show the localized states of the Fe^{3+} ions in the tetrahedral and octahedral sublattices. These states are given according to crystal field calculations which take into account tetragonal distortions in the tetrahedral sublattice and trigonal distortions in the octahedral sublattice [18].The calculations show that the relevant splittings and shifts of the electronic states may of the order of 0.5 eV and therefore comparable to the splitting of the states in the cubic crystal fields of T_d and O_h symmetry.

Below the band gap the electronic transitions could be studied by transmission methods based on optical and magneto-optical techniques, whereas for transitions above the band gap of ≈ 3.2 eV reflection methods are in general more favorable [9,11,12]. With the use of very thin YIG films (t = = 0.26 μm) absorption spectra could be obtained up to 5.0 eV [6]. It should be noticed that all optical transitions between the localized states of the Fe^{3+} ions are spin-forbidden. In addition, the transitions in the octahedral sublattice are parity-forbidden in the electric-dipole approximation and become allowed due to interaction with odd phonons.

Optical absorption of YIG in the near infrared spectral range commences at about 1.2 eV and is due to the localized electronic transition $^6A_{1g} \rightarrow {}^4T_{1g}$ between the $(3d)^5$ levels of the Fe^{3+} ions in the octahedral sublattice. This transition is magnetic-dipole-allowed and leads to two very

weak absorption lines [10]. It is readily seen from Fig. 1 that at higher energy the transitions in the octahedral and the tetrahedral sublattices are overlapping, so that the unambiguous assignment of the states becomes difficult. In fact, the experimentally observed spectrum of YIG is characterized by a more complicated structure than expected from theory even if the case of very low symmetries is taken into account. Aside from their dependence on the cubic and noncubic crystal field parameters, the positions of the electronic levels are also subject to several other parameters, such as the intra-atomic interaction parameters, spin–orbit coupling, exchange interaction, etc. In strongly correlated systems like iron garnets, paired transitions may lead to additional absorption bands in the optical spectra. For example, absorption bands in the spectral range around 2.5 eV are at least in part due to paired transitions. These factors, being sometimes of comparable magnitude or not exactly known, complicate the unique assignment of optical absorption bands. Low-temperature optical and magneto-optical studies resolve the splittings of the transitions, revealing a rather complicated energy-level structure.

The exact position of the band gap remains not well defined and is usually assumed to lie near 3.2–3.4 eV, where the absorption coefficient of YIG starts to increase more rapidly, approaching values of $\alpha = 5 \cdot 10^5$ cm^{-1} above 5 eV [6]. This absorption value is typical for interband transitions in transition-metal oxides. The substitution of Bi^{3+} for Y^{3+} in iron garnets leads to a shift of the strong absorption edge to lower energy and to a huge increase of magneto-optical effects in the visible and ultraviolet spectral range. The suggested microscopic mechanisms of the enhanced magneto-optical Faraday and Kerr effects are assumed to originate in an increase of the spin–orbit interaction due to the formation of a molecular orbit between the 3*d* orbitals of the Fe^{3+} ions and the 2*p* orbitals of O^{2-}. This is further mixed with the 6*p* orbitals of Bi^{3+}, which has a large spin–orbit interaction coefficient. A recent analysis shows that the most important electronic transitions responsible for the Faraday rotation in bismuth-substituted garnets lie at 2.6, 3.15, and 3.9 eV [19].

3. Experiment

In the present study we used thin films of magnetic garnets grown by a liquid-phase epitaxial method. Films were grown on transparent nonmagnetic substrates cut from bulk cubic crystals of gadolinium gallium garnet $Gd_3Ga_5O_{12}$ or substituted GGG. The films were grown on substrates with the four different orientations (001), (110), (111), and (210) and differed in their compositions, lattice parameters, and thicknesses [8]. Optical absorption spectra were measured using a Cary 2300 spectrophotometer and were found to be in agreement with published data. Absorption spectra measured at T = 15 K in three films are shown in Fig. 2. Optical densities higher than $D = 4.5$ are above the working range of the spectrophotometer and could not be measured.

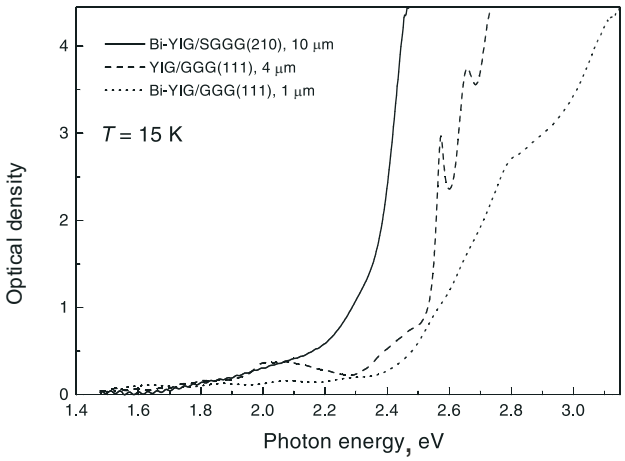

Fig. 2. Optical absorption spectra in the three garnet films studied in the paper. The films differ in their compositions and thicknesses. Optical densities higher than $D = 4.5$ are out of the range of the spectrophotometer and could therefore not be measured.

The setup for the SHG and THG experiments is shown in Fig. 3. A Nd: YAG laser system and a β-BaB_2O_4 operated optical parametric oscillator

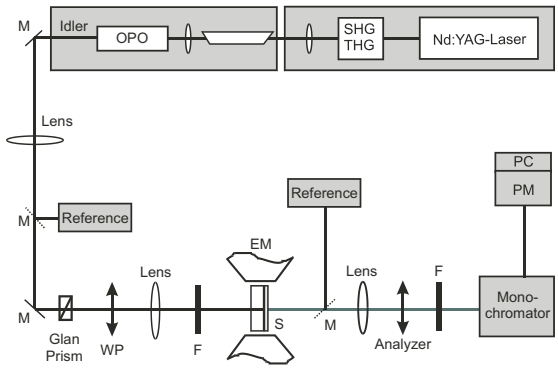

Fig. 3. Transmission setup for SH/TH spectroscopy. SHG/THG: second harmonic/third harmonic generation; OPO: optical parametric oscillator; WP: wave plate; F: filter; S: sample; EM: electromagnet; PM: photomultiplier; PC: personal computer; M: mirror.

(OPO) were used as the light source, the performance of which was monitored with a wavemeter. The pulse energy was measured for normalizing the observed SH and TH intensities. For proper normalization it was necessary to measure the absorption of the fundamental beam by placing a photodiode behind the sample, since in all samples the absorption varies strongly as function of the photon energy. Wave plates, polarizers, and optical filters were used to set the polarization of the fundamental light, analyze the polarization of the SH and TH light, and separate the fundamental light from the SH and TH light behind the sample. In some cases, a monochromator was included in the setup in order to exclude the possibility of two-photon luminescence contributions to the observed signals. By a telephoto lens the signal light was projected on a cooled CCD camera or a photomultiplier. The data were corrected for the spectral response of the filters and the detection system. The magnetic contrast was determined from the normalized difference between the SH intensity for opposite orientations of the saturating transverse magnetic field.

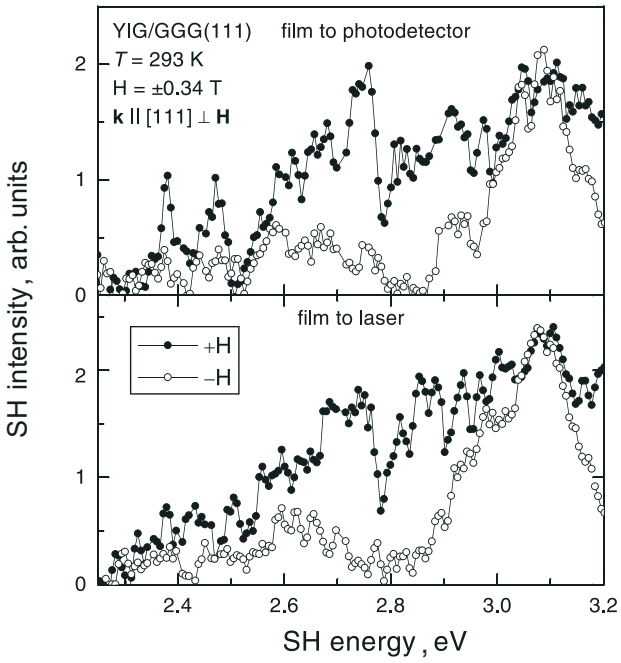

Fig. 4. SH spectra in the YIG/GGG(111) film for opposite orientations of the transverse magnetic field. The upper and lower panels depict SH spectra for two sides of the film.

4. Nonlinear optical susceptibilities

In magnetically ordered materials the relation between the induced polarization **P** and the electric field **E**(ω) of the fundamental beam in the electric dipole approximation can be written as

$$\mathbf{P} = \varepsilon_0(\hat{\chi}^{(1)}\mathbf{E}(\omega) + \hat{\chi}^{(2)}\mathbf{E}(\omega)\mathbf{E}(\omega) + \hat{\chi}^{(3)}\mathbf{E}(\omega)\mathbf{E}(\omega)\mathbf{E}(\omega)\ldots). \quad (1)$$

In the electric-dipole approximation, odd tensors $\hat{\chi}^{(1)}, \hat{\chi}^{(3)}, \ldots$ are allowed in all media, whereas even tensors $\hat{\chi}^{(2)}, \hat{\chi}^{(4)}, \ldots$ are allowed only in noncentrosymmetric media. For crystals with a spontaneous or a magnetic-field-induced magnetization **M** the optical susceptibility tensors contain crystallographic (nonmagnetic) contributions and magnetic contributions:

$$\hat{\chi}^{(n)} = \hat{\chi}^{\mathrm{cr}} + \hat{\chi}^{m}\mathbf{M}\,. \quad (2)$$

The intensity of SH and TH signals can be written as

$$I(2\omega) \propto E_0^4 |\hat{\chi}^{\mathrm{cr}}(-2\omega;\omega,\omega) \pm \hat{\chi}^{m}(-2\omega;\omega,\omega,0)M|^2\,,$$
$$I(3\omega) \propto E_0^6 |\hat{\chi}^{\mathrm{cr}}(-3\omega;\omega,\omega,\omega) \pm \hat{\chi}^{m}(-3\omega;\omega,\omega,\omega,0)M|^2\,, \quad (3)$$

Table

Nonzero components of the nonlinear optical tensors $\chi^{\mathrm{cr}}_{ijkl}$ and χ^{m}_{ijklm} relevant for the point group $3m$ ($m \perp x$) in the geometry $\mathbf{k} \| \mathbf{z}$ (films of (111) type)

$\chi^{\mathrm{cr}}_{ijkl}$	χ^{m}_{ijklm}
$\frac{1}{3}yyyy = \frac{1}{3}xxxx = xxyy = yxxy$	$yyyyx,\ yxyyy,\ yxxyx$ $xxxxx = -\frac{1}{2}yyyyx - yxyyy - \frac{1}{2}yxxyx$ $xxxyy = \frac{1}{2}yyyyx - \frac{1}{2}yxxyx$ $xxyyx = -\frac{1}{2}yyyyx + yxyyy - \frac{1}{2}yxxyx$ $xyyyy = \frac{1}{2}yyyyx + yxxyx$ $yxxxy = yyyyx - yxyyy + yxxyx$ $yxyyz = -xxxyz = -\frac{1}{3}xyyyz = \frac{1}{3}yxxxz$

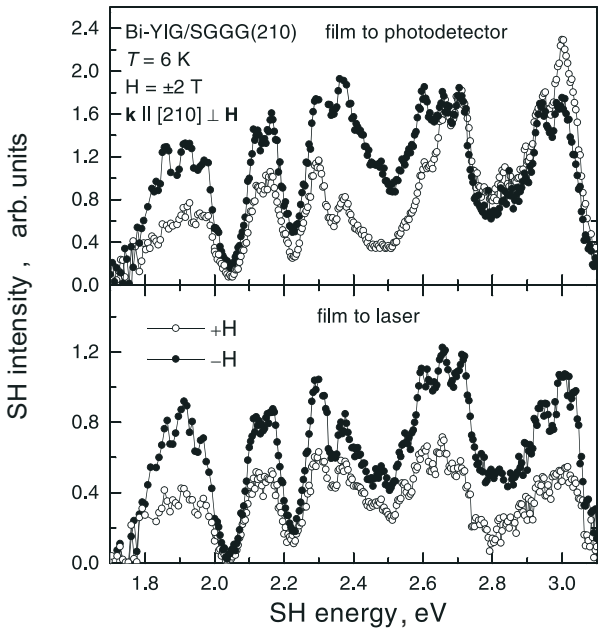

Fig. 5. SH spectra in the Bi-YIG/SGGG(210) film.

where the crystallographic and magnetic contributions are described by polar tensors $\hat{\chi}^{cr}$ and axial tensors $\hat{\chi}^{m}$, respectively. The sign ± refers to the opposite projections of the magnetization **M**. The symmetry properties of the tensors $\hat{\chi}^{cr}$ and $\hat{\chi}^{m}$ are strictly defined by the crystallographic point group. Nonzero components of $\hat{\chi}^{cr}$ and $\hat{\chi}^{m}$ are given in Ref. 8 for SHG and in Table for THG for the case of 3*m* symmetry. If nonlinear optical waves of crystallographic and magnetic origin are both present, their interference will lead to different SH and TH intensities for opposite orientations of the magnetization and thus to a magnetic contrast between oppositely magnetized regions.

5. Experimental results and discussion

Figure 4 shows the SH spectra in a YIG/GGG (111) film for two opposite orientations of the magnetization **M** in transverse geometry. The upper and lower panels show the results for the two cases with the SH signal being emitted directly from the free film surface (film-to-photodetector case) and from the surface of the film attached to the substrate (film-to-laser case). The two geometries lead to different SH spectra. In particular, a split transition near 2.4 eV is well resolved for the free film surface and smeared out for the more strained surface attached to the substrate. Note that magnetic contrast varies from 0 to 100%. According to the energy level diagram in Fig. 1, some features in the SH spectrum can be assigned to the crystal-field transitions in the two iron sublattices. Two other sharp absorption features near 2.57 eV (presumably due to the ${}^6A_1 \rightarrow {}^4E,\ {}^4A_1$ transition in the tetrahedral sublattice) and 2.66 eV (presumably due to the ${}^6A_1 \rightarrow {}^4E,\ {}^4A_1$ transition in the octahedral sublattice) are also observed in the SH spectrum. Two more spectral features in the absorption spectrum are observed at 2.9 and 3.2 eV, with oscillator strengths an order of magnitude higher than those for the tetrahedral transitions. However, the relevant features in the SH spectrum are of the same order of magnitude as for the transitions with the lower optical absorption.

Figure 5 shows the SH spectra of a bismuth-substituted Bi-YIG/SGGG(210) film. As a rule bismuth-substituted films show the strongest SH signals [8]. The present sample was studied in a spectral range beginning at 1.7 eV and at low temperature $T = 6$ K. It shows a well-resolved structure with five strong bands of varying magnetic contrast. We note that the spectra for two sides of the film are different, as it was the case for the YIG/GGG(111) film. As in the previous case, the increase of the linear optical absorption does not lead to a noticeable increase of the SH intensity.

Figure 6 shows the third harmonic spectra in the three magnetic films. Note that even in the elec-

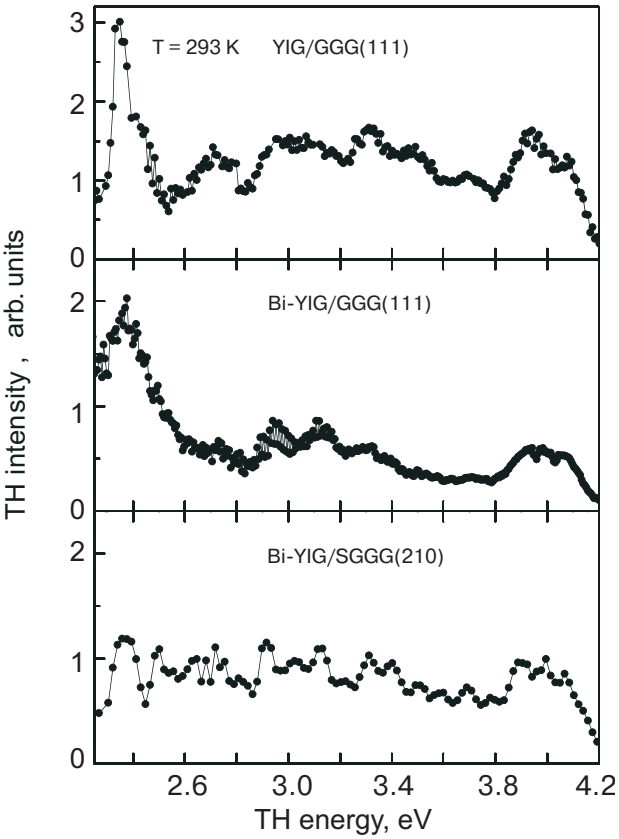

Fig. 6. TH spectra in YIG/GGG(111), Bi-YIG/GGG(111), and Bi-YIG/SGGG(210) films.

tric-dipole approximation a breaking of space inversion symmetry is not required for the observation of a TH signal. Although the optical absorption and the magnitudes of the linear magneto-optical signals are very different in the three films, their third harmonic spectra are similar. The tetrahedral transition $^6A_1 \rightarrow {}^4T_2$ centered near 2.4 eV is well resolved in the TH spectrum, and in particular in the YIG/GGG(111) film. Note that the strong increase of the linear absorption above 3 eV is not accompanied by a similar increase of the TH spectra. Contrary to the SH spectra, no difference in the TH spectra is observed within the experimental accuracy upon a reorientation of the magnetization or upon a variation of the magnetic field. This is surprising, because according to a phenomenological analysis a magnetic contribution to the THG is allowed both in the longitudinal and transverse geometries.

In conclusion, the SH spectra of various anisotropic magnetic garnet films were measured in a range of photon energies stretching from 1.7–3.2 eV and thus, below the fundamental band gap at ≈ 3.2 eV. The spectra revealed contributions of nonmagnetic and magnetic type to the total SH intensity. We also report the TH spectra in the range of 2.4–4.2 eV and thus, below and above the band gap. No studies along these lines for the magnetic transition-metal oxides have been reported so far with the only recent exception of third harmonic spectroscopy of La_2CuO_4 [20]. While the intensity of linear absorption grows progressively as a function of photon energy, the intensity of the SH and TH spectra does not show a similar behavior. We may assume that this is due to the fact that only localized d–d transitions contribute to the nonlinear spectra, with the relevant contribution vanishing for charge-transfer and interband transitions. A very interesting and puzzling result is the observation of a very large magnetic contribution to the SH spectra with a magnetic contrast of up to 100%. By contrast, no magnetic contribution is found in the TH spectra. All these observations demonstrate a strong necessity for further experimental and theoretical studies of nonlinear optical properties of magnetic garnet materials.

6. Acknowledgments

This work was supported by the Deutsche Forschungsgemeinschaft, the Russian Foundation for Basic Research, and the Alexander-von-Humboldt-Stiftung. We thank H.-J. Weber for the help in optical absorption measurements.

1. *Physics of Magnetic Garnets*, A. Paoletti (ed.), North Holland, Amsterdam (1978).
2. G. Winkler, *Magnetic garnets*, Vieweg, Braunschweig (1981).
3. *Magnetic garnet films*, A. Paoletti (ed.), special issue of *Thin Solid Films* **114** (1984).
4. Landolt-Börnstein, *Numerical Data and Functional Relationships in Science and Technology*, New Series, Group III, 27/e, Springer-Verlag, Berlin (1991).
5. D. L. Wood and J. P. Remeika, *J. Appl. Phys.* **38**, 1038 (1967).
6. G. B. Scott and J. L. Page, *Phys. Status Solidi* **B79**, 203 (1977).
7. B. B. Krichevtsov, V. V. Pavlov, and R. V. Pisarev, *JETP Lett.* **49**, 535 (1989); *Sov. Phys. Solid State* **31**, 1142 (1989).
8. V. N. Gridnev, V. V. Pavlov, R. V. Pisarev, A. Kirillyuk, and Th. Rasing, *Phys. Rev.* **B63**, 184407 (2001) and references therein.
9. F. J. Kahn, P. S. Pershan, and J. P. Remeika, *Phys. Rev.* **186**, 891 (1969).
10. J. P. van der Ziel, J. F. Dillon, Jr., and J. P. Remeika, *AIP Conf. Proc.* **5**, 254 (1971).
11. A. I. Galuza, V. V. Eremenko, and A. P. Kirichenko, *Sov. Phys. Solid State* **15**, 407 (1973).
12. K. W. Blazey, *J. Appl. Phys.* **45**, 2273 (1974).
13. S. H. Wemple, S. L. Blank, J. A. Seman, and W. A. Biolsi, *Phys. Rev.* **B9**, 2134 (1974).
14. G. B. Scott, D. E. Lacklison, and J. L. Page, *Phys. Rev.* **B10**, 971 (1974).
15. B. B. Krichevtsov, O. Ochilov, and R. V. Pisarev, *Sov. Phys. Solid State* **25**, 1380 (1983).
16. T. K. Vien, J. L. Dormann, and H. Le Gall, *Phys. Status Solidi* **71**, 731 (1975).
17. A. S. Moskvin, A. V. Zenkov, E. I. Yuryeva, and V. A. Gubanov, *Physica* **B168**, 187 (1991).
18. V. V. Alekseev, V. V. Druzhinin, and R. V. Pisarev, *Sov. Phys. Solid State* **33**, 1507 (1991).
19. G. F. Dionne and G. A. Allen, *J. Appl. Phys.* **73**, 6127 (1993).
20. A. Schülzgen, Y. Kawabe, E. Hanamura, A. Yamanaka, P.-A. Blanche, J. Lee, H. Sato, M. Naito, N. T. Dan, S. Uchida, Y. Tanabe, and N. Peyghambarian, *Phys. Rev. Lett.* **86**, 3164 (2001).